Biosensors and Bioelectronics 127 (2019) 161–166

Contents lists available at ScienceDirect

Biosensors and Bioelectronics

journal homepage: www.elsevier.com/locate/bios

Target-inspired Zn^{2+}-dependent DNAzyme for ultrasensitive impedimetric aptasensor based on polyacrylic acid nanogel as amplifier

Juncai Zhao, Di Shu, Zhanfang Ma*

Department of Chemistry, Capital Normal University, Beijing 100048, China

ARTICLE INFO

Keywords:
Impedimetric aptasensor
Carcinoembryonic antigen
DNAzyme
Polyacrylic acid nanogel

ABSTRACT

In general, the traditional impedimetric aptasensor for detecting protein is based on its high molecular weight and low dielectric constant. Yet, the efficiency of these aptasensors is hindered by the slight resistance change in the trace concentration range because of the high initial resistance (the electrostatic repulsion between the compact negatively charged DNA on the electrode and $[Fe(CN)_6]^{3-/4-}$). To effectively and simply circumvent this issue and improve the detection sensitivity, we design an impedimetric aptasensor by reducing the substrate DNA's density on the electrode through the target-inspired recycling DNA cleavage. In order to enlarge the differences in resistance, the polyacrylic acid (PAA) nanogel is implemented as amplifier due to its poor conduction and negative charge that can hinder electron transfer and repulse the mediator $[Fe(CN)_6]^{3-/4-}$, respectively. Based on the target-inspired DNAzyme and PAA nanogel as amplifier, the ultrasensitive impedimetric aptasensor of carcinoembryonic antigen (CEA) in the buffer solution possesses a wide dynamic range of 10 fg mL^{-1} to 10 ng mL^{-1} and ultra-low detection limit of 7.9 fg mL^{-1} (10-fold relative to equivalent aptasensors). When tested in human serum, the proposed aptasensor exhibits good performance with an ultra-low detection limit of 1.4 fg mL^{-1}, which is slightly higher than that in buffer solution.

1. Introduction

Exploring biosensors for the sensitive detection of important biomarkers is of permanent interest for early disease diagnosis, treatment, and management (Chinen et al., 2015). Generally, biosensing systems are composed of two basic elements, one for biomolecule recognition and the other for signal readout (Chen et al., 2017; Chandra, 2016). Hence, the main impetus of biosensing research is focused on searching highly selective recognition and developing facile signal transduction pathways for the sensitive detection of target biomarkers. Among the signal readout techniques, the electrochemical method possesses innate advantages of high sensitivity, rapid response, simplicity and low-cost fabrication (Zhao and Ma, 2018). Compared with differential pulse voltammetry and square wave voltammetry, electrochemical impedance spectroscopy (EIS) technique can be implemented as a redox marker-free detection method and has high sensitivity in a low protein concentration range (Deng et al., 2009; Park et al., 2008). Therefore, EIS has become an effective technique for signal readout of biomarkers, especially protein (Deng et al., 2009; Park and Park, 2009).

Functional nucleic acid (FNA), which possesses prominent nature in precisely replicating creatures and specificly recognizing biomarkers, attracts the attention of researchers (Liu et al., 2009; Chandra et al., 2011; Song et al., 2008). Up to now, FNA has been regarded as an efficient sensing element that can be integrated in numerous biosensors (Zhang et al., 2013; Gao et al., 2017; Li et al., 2018; Xu et al., 2015; Lee et al., 2014). An example of such biosensor is based on DNA-stabilized silver nanoclusters, which is used to detect dopamine by using fluorescent (Del Bonis-O'Donnell et al., 2018). Other biosensors include an electrochemical aptasensor to detect cocaine in whole blood (Li et al., 2016) and a fluorescent DNA aptazyme sensor based on target-induced unfolding of DNA hairpins (Zhou et al., 2015). In particular, aptamers, nucleic acid probes generated from SELEX (Dunn et al., 2017; Her et al., 2017; Choi and Ban, 2016), are a particularly attractive recognition element to design different affinity-based aptsensors without the involvement of any signal amplification strategies and nanomaterials (Zhai et al., 2016; Liu et al., 2015). However, the sensitivity of such aptamers is limited, despite their simplicity. To improve the sensitivity, diverse combination modes containing aptamers and other FNA chains have been extensively utilized in aptasensors, such as the aptamer-cleavage DNAzyme (Zhong et al., 2018), aptamer-peroxidase mimicking DNAzyme (Zhou et al., 2017; Wu et al., 2018) and aptamer-template DNA for preparing nanoparticles (Guo et al., 2017; Yang et al., 2015). Indeed, these modes can extensively improve the sensitivity and decrease the detection limit down to about 0.1 pg mL^{-1}. The majority

* Corresponding author.
E-mail address: mazhanfang@cnu.edu.cn (Z. Ma).

https://doi.org/10.1016/j.bios.2018.12.030
Received 1 September 2018; Received in revised form 27 November 2018; Accepted 16 December 2018
Available online 21 December 2018
0956-5663/

of them can be realized with the help of multistep hybrid nanomaterial synthesis (the carrier of the functional DNA and signal generation), probe conjugations or modifications on the nanomaterials and the extra additive for signal amplification, which compromises the simplicity of aptasensor. Considering that nanomaterial synthesis and modification involve the time-consuming and tedious multistep separation, purification, and washing processes, the development of a simple and effective method for sensitive detection is highly urgent.

Polyacrylic acid (PAA) nanogel, an anionic hydrogel with good flexibility, biocompatibility, easy preparation and hydrophilicity, has a potential as probe in biosensors (Al-Sagur et al., 2017). It is well-known that PAA is a negatively charged polyelectrolyte that can provide abundant carboxylic groups to fix amino-modified DNA via an esterification reaction between the surface amino groups of DNA and the carboxylic acid group of PAA. In addition, the poor conductivity and negative charge of PAA can respectively hinder the electron transfer of redox mediators and repulse mediators, which increase the charge transfer resistance, thus suggesting the potential of PAA nanogel as a resistance amplifier in imedimetric biosensors (Mawad et al., 2016). Aptazyme is a single-strand DNA (integration between an aptamer and cleavage DNAzyme), where the DNAzyme activity is modulated by the aptamer binding to the target analyte (Zhou et al., 2015; Ali and Li, 2009; Liu and Lu, 2004). It also innately exhibits the recognition and amplification capabilities without the involvement of any nanomaterials, modification or extra reagents. In addition, aptazyme can undergo turnovers many times without losing its binding ability and catalysis activity. Based on these merits of aptazyme, herein, an ultrasensitive impedimetric aptasensor is designed by combining the aptazyme and PAA nanogel as amplifier in this work. In the proposed strategy, the hairpin structure of the aptazyme is forced open, recovering the activity of cleavage DNAzyme in the presence of the target. The activated DNAzyme can circularly cleave the corresponding substrate on the electrode to reduce resistance. Implementing the poorly conductive and negatively charged PAA nanogel as the amplifier in this method increases the difference in resistance, and an ultra-low detection limit of 7.9 fg mL^{-1} (about 10-fold relative to equivalent aptasensors) can be subsequently obtained. The designed aptasensor possesses the following characteristics: (1) The introduction of the tandem reaction can remarkably improve the detection sensitivity and offer a new approach to incorporate aptazyme with an impedimetric aptasensor. (2) The tandem reaction without extra reagents, i.e. the target recognition and DNA cleavage process, can simplify the operation and shorten the analytic time. (3) To further improve the sensitivity, the poor conductivity and negative charge of PAA nanogel can hinder the electron transfer and repulse the mediator $[Fe(CN)_6]^{3-/4-}$, respectively, which can tremendously amplify the difference in resistance. To testify the validity of the ultrasensitive aptasensor, carcinoembryonic antigen is chosen as the model biomarker since its detection is of significance in the diagnosis of breast, lung and rectal cancers (Ren et al., 2017).

2. Experimental section

2.1. Reagents and apparatus

All oligonucleotides were synthesized and purified via HPLC by Sangon Biotechnology Co. Ltd. (Shanghai, China) (The sequence of oligonucleotides is displayed in Table S1.). Tris(2-carboxyethyl) phosphine hydrochloride (TCEP), (N-hydroxysuccinimide) (NHS), (1-ethyl-3-[3-dimethylaminopropyl] carbodiimide hydrochloride) (EDC), 6-mercaptohexanol (MCH), were purchased from the Sigma-Aldrich. Carcinoembryonic antigen (CEA), neuron specific enolase (NSE) and prostate specific antigen (PSA) were attained by Shanghai Linc-Bio Science Co. Ltd (Shanghai, China). Human immunoglobulin G (IgG) was achieved from Beijing Xinjinke Bioechnology Co. Ltd. (Beijing, China). Sodium dodecyl sulfate (SDS) was bought from Thermo Fisher Scientific (China). Acrylic acid (AA), N,N′-methylenebisacrylamide (MBA) and ammonium persulfate were obtained from Sinopharm Chemical Reagent Co. Ltd (China). All other reagents were of analytical pure and used without further purification. All the solutions were prepared by using the deionized water. All the buffer solutions were used as follows: Buffer A (1 M NaCl and 10 mM phosphate buffer (pH 7.4)) was used undermentioned experiment except special requirement. Buffer B contained 1 M NaCl, 1 mM Mg^{2+}, 0.1 mM Zn^{2+} and 10 mM phosphate buffer (pH 7.4) as cleavage buffer (Mg^{2+} can stabilize the aptazyme hairpin structure (Anthony et al., 2012)).

Electrochemical measurements were carried out by a multichannel potentiostat (VMP3, France) at ambient temperature. A three-electrode system consisted of a gold electrode (GE, Φ = 4 mm) as the working electrode, an Ag/AgCl electrode (saturated KCl) as reference electrode and a Pt wire as counter electrode.

The morphology of PAA nanogel was characterized by A JEOL-100CX transmission electron microscope (TEM) (H7650, Hitachi, Japan). X-ray photoelectron spectroscopy (XPS) (Thermofisher, American,) and energy dispersive X-ray spectrometer (EDS) (Hitachi SU8010) were used to analyze the element of composites.

2.2. Gold electrode pretreatment and modification

Gold electrode was carefully polished to a clean surface with 0.05 μm alumina powders for 5 min and sonicated in ethanol and ultrapure water respectively (Zhao and Ma, 2018). Then electrode was activated by electrochemical cleaning with successive cyclic voltammetry scans from −0.4 V to + 1.2 V (vs. saturated calomel electrode) in 0.5 M H_2SO_4 at 100 mV s^{-1} to stable (Liu et al., 2015). Subsequently, the electrode was incubated with 250 nM thiolated substrate DNA at 37 °C overnight pretreated with 25 μM TCEP (Buffer A) for one hour. After the electrode surface was then rinsed three times with buffer A, the surface was passivated with 1 mM MCH for an hour at the ambient temperature. The modified electrode was stored in buffer A prior to measurement.

2.3. Synthesis of the PAA/Link nanogel

The PAA nanogel was synthesized according to the literature with a great modification (Shaik et al., 2016). Briefly, the mixture solution of the 0.5 mL pristine HNO_3, 50 mg SDS and 60 mg ammonium persulfate contained 55 mL H_2O was quickly stirred for 10 min. Then, the polymerization reaction was initiated by the adding the mixture of 50 mg MBA and 1 mL AA under the 80 °C bath. After the 80 °C for 4 h, the PAA nanogel was prepared. The solution was centrifuged twice to remove unreacted reagents and was re-dispersed into 11 mL H_2O for further use. Before the conjugation Link DNA with amino group, the 2 mL fresh EDC and NHS (0.2 M) was injected into the 2 mL PAA nanogel in 37 °C for 1 h in order to activate carboxyl group. The active PAA nanogel was centrifuged once to 2 mL PBS and 10 μL 100 μM Link DNA was added into the above solution in 37 °C for 2 h. The solution was centrifuged and was stored in 2 mL PBS in 4 °C.

2.4. Impedimetric detection of CEA

The mixture of 250 nM aptazyme and different CEA concentrations (buffer B) was dropped into the modified electrode at 40 °C for 1 h. After rinsed three times with buffer A, the electrode was incubated with the 20 μL PAA/Link nanogel at 37 °C for 1 h. Following that, the signal readout was recorded by the electrochemical impedance spectroscopy (EIS). EIS measurement was performed in 5 mM $K_3[Fe(CN)_6]/K_4[Fe(CN)_6]$ (1:1) containing 0.1 M KCl under the following conditions: the applied potential at 0 V versus open circuit voltage, the alternative voltage amplitude of 10 mV and the voltage frequencies ranging from 100 kHz to 0.02 Hz.

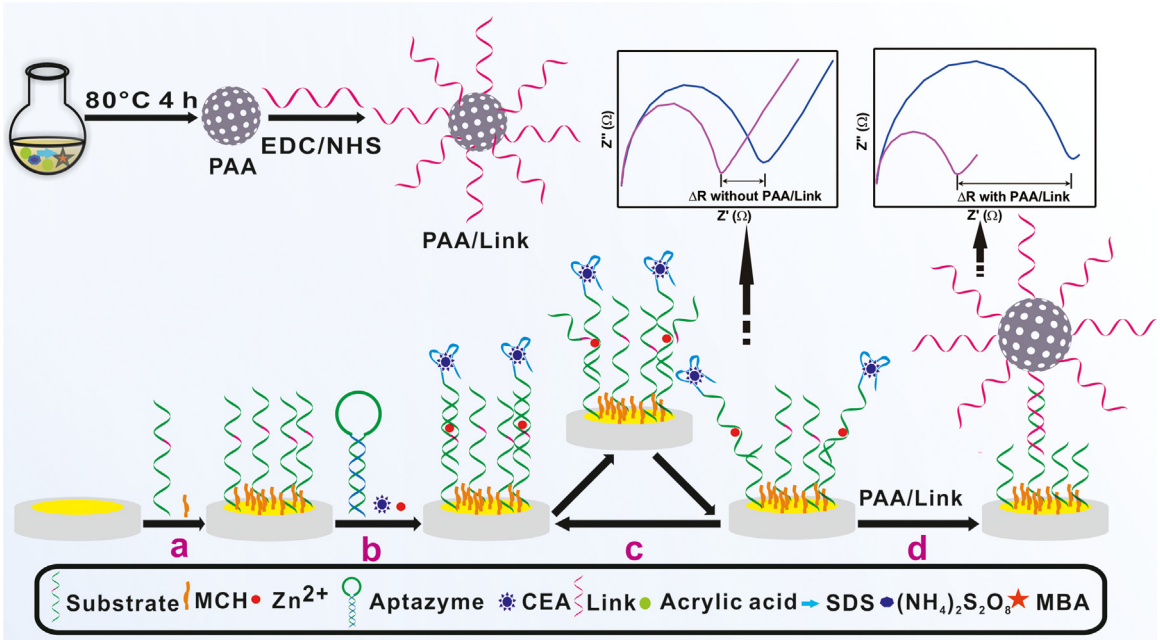

Scheme 1. Preparation of ployacrylic acid (PAA) nanogel, Schematic illustration of fabrication of the impedimetric aptasensor for CEA detection and the amplification effect of PAA/Link nanogel.

3. Results and discussion

3.1. Principle of designed impedimetric aptasensor

For the impedimetric aptasensor, the charge transfer resistance (R_{ct}) is generated by the electrostatic repulsion between the negatively charged DNA and negative charge of the mediator ($[Fe(CN)_6]^{3-/4-}$) (Wang et al., 2017). However, the trace proteins induce the negligible increase in R_{ct} due to a high initial R_{ct} ascribed to high DNA density on the electrode, which is an obstacle for the sensitive detection in impedimetric aptasensor. In contrast, if the trace proteins cause a decrease in R_{ct}, the high initial R_{ct} is beneficial for the sensitive detection in impedimetric aptasensor. Therefore, introduction of the target-inspired DNAzyme can render that the R_{ct} is inversely proportional to the concentration of the target.

The principle of the detection procedure is illustrated in Scheme 1. The thiolated substrate strand for Zn^{2+} DNAzyme with a ribonucleotide adenosine in the scissile position (red dot) is immobilized onto the gold electrode (a). Although Pb^{2+} is accepted to be more selective toward 8–17 DNAzymes in catalytic effect for the designed DNAzyme, Zn^{2+} owns lower toxicity and better solubility (Schlosser and Li, 2010). Therefore, Zn^{2+} is chosen as a cofactor of the DNAzyme. Aptazyme, the hairpin DNA containing the enzyme cleavage strand (DNAzyme) and recognition strand of CEA (aptamer), can block the activity of the enzyme strand by intramolecular hybridization. When CEA is present, it can bind to the aptamer and concomitantly recover the activity of the DNAzyme (b). Then, with the assistance of Zn^{2+}, the activated DNAzyme can catalyze the cleavage of its substrate strand on the electrode surface (c), which reduces the density of the substrate strand on the electrode surface and decreases the charge transfer resistance (R_{ct}). In other words, the density of the substrate strand on the electrode surface depends on the number of activated DNAzymes that are affected by the concentration of the target. In addition, poorly conductive and negatively charged polymer (PAA/Link nanogel), as an amplifier, can be conjugated to the substrate strand on the electrode surface (d) in order to enlarge differences between the R_{ct} with target and without target, which is ascribed by effective block the electron transfer to the electrode and the repulsion between the electrode surface and the negatively charged redox indicator ions ($[Fe(CN)_6]^{3-/4-}$) (the high density of substrate strand can fix a mass of PAA/Link nanogel and vice versa). Therefore, differences in R_{ct} are significantly increased upon CEA binding event, rendering to an ultra-low detection limit.

3.2. Characterization of PAA and PAA/Link nanogel

The TEM images revealed that the average diameter of the PAA nanogel was about 150 nm (Fig. 1**A**). The elements of the PAA and PAA/Link nanogel were analyzed with XPS (Fig. 1**B**) and EDS (Fig. S1). The EDS analysis revealed that C and O atoms exist in the PAA nanogel in Fig. S1A. Compared with the PAA nanogel, the PAA/Link nanogel contains P atoms, indicating the successful modification of Link DNA on the PAA nanogel due to the phosphate groups in the DNA structure (Fig. S1B). The XPS spectrum of the PAA nanogel presented peaks at 284.8 and 532.5 eV, which were attributed to C 1s and O 1s, respectively (Fig. 1**B**), while the spectrum of the PAA/Link nanogel revealed additional peaks at 400.3 and 133.0 eV. The results indicated that Link DNA was successfully ligated to the PAA nanogel because the DNA structure contains N and P elements.

3.3. EIS and SWV characterization of stepwise procedures of the aptasensor

As shown in Fig. 2, the entire modification procedures were monitored by EIS and square wave voltammetry (SWV). In Fig. 2**A**, compared with the R_{ct} of the bare gold electrode (a), a large R_{ct} was obtained for the substrate DNA and MCH-modified electrode (b) due to the electrostatic repulsion between negative charges of DNA and the negatively charged redox indicator ions. The R_{ct} continued to remarkably increase after the incubation of CEA and aptamer-enzyme DNA (c), elucidating that the hairpin structure is opened by CEA. Subsequently, the R_{ct} significantly decreased with the aid of the Zn^{2+} (d). When the PAA/Link nanogel was successfully ligated to the above electrode (e), the R_{ct} increased, which may be attributed to the electrostatic repulsion and poor conductivity of the PAA/Link nanogel. In Fig. 2**B**, compared to the current of the bare gold electrode (a), the current of the substrate DNA and MCH-modified electrode (b) greatly decreased, which indicates the successful modification of substrate DNA and MCH on the electrode. To validate the aptamer-target binding and DNAzyme cleavage, the current decreased after adding CEA (c) due to

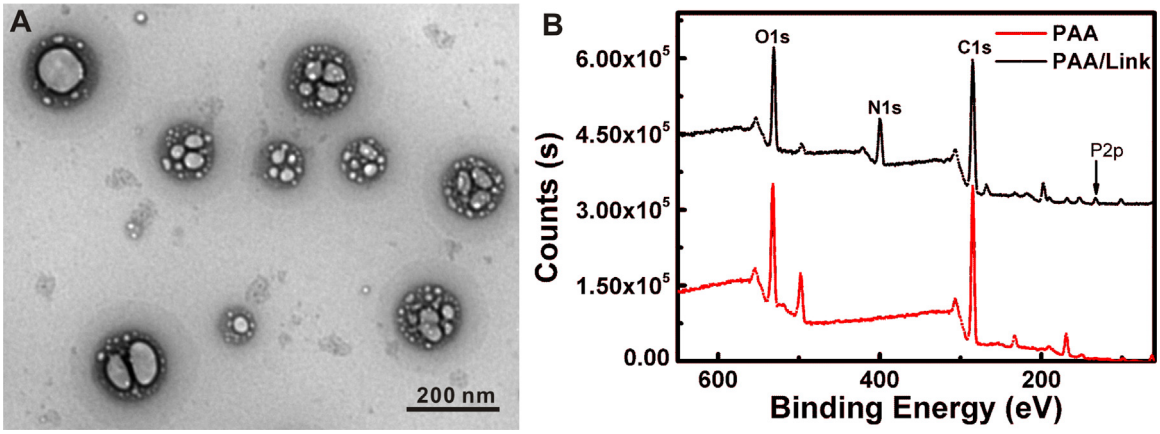

Fig. 1. TEM image of PAA nanogel (A) and XPS spectra for PAA (red line) and PAA/Link nanogel (black line).

its high molecular weight and low dielectric constant. The current subsequently increased with the aid of Zn^{2+} (d) because the substrate DNA on the electrode was cleaved and released from the electrode. Upon incubation of PAA/Link nanogel, the current (e) was reduced, inferring that the PAA/link nanogel was fixed on the electrode. The results of SWV (Fig. 2**B**) were consistent with that of EIS (When the R_{ct} increases, the peak current decreases, and vice versa.). In additional, to further validate the aptamer-target binding event and DNAzyme cleavage event, gel electrophoresis was used (the detailed information in the Supplement Material). Only in the mixture containing the aptazyme, substrate and CEA (4), the strip of cleavage product was obviously observed in the inset of Fig. S2B (PAGE image), indicating that the apatamer-target binding and DNAzyme cleavage occurs. Consequently, the results well proved the processes of the aptasensor.

3.4. Feasibility of designed aptasenor

To evaluate the feasibility of the tandem reaction, we first ensured that the aptamer-enzyme strand (hairpin) can recognize the CEA, and that the opened hairpin can hybridize with the substrate DNA in the electrode (blue) (Fig. S2A). Then, we investigated that substrate was cleaved in the presence of Zn^{2+} (black). In order to verify this process, it was pertinent to find a moderate cleavage temperature at which the opened hairpin can be dissociated from the splitting fragment in the electrode. Therefore, a series of cleavage temperatures were analyzed in Fig. 3**A**. The difference in R_{ct} increased as the cleavage temperature increased and then was a trend to lower slightly at 42 °C (the RSD of 42 °C is 48%, which indicated the unstability of the method under the 42 °C.), which was mainly attributed to the equilibrium between the recognition of CEA and cleavage ability. The experimental results were coherent with those calculated using the Oligo Analyzer (Supplement material). In addition, to confirm the amplification effect of the PAA/Link nanogel, changes in R_{ct} with and without the PAA/Link nanogel under the same conditions was investigated in Fig. S2B. Obviously, the difference in R_{ct} with PAA/Link nanogel was much larger than that without PAA/Link nanogel, which validated the amplification effect of the PAA/Link nanogel.

3.5. Optimization of concentration of substrate DNA, cleavage temperature and recycling time

The number of substrates and extent of amplification during the recycling step (the tandem reaction) directly depended on the concentration of the substrate DNA that was effectively assembled onto the electrode surface. The $-\Delta R_{ct}$ value ($\Delta Rct = R\text{-}R_0$; R and R_0 denote the charge transfer resistance with target and without target after incubation of PAA/Link nanogel, respectively) was used as an assessment standard. $-\Delta R_{ct}$ was the largest when the concentration of substrate DNA was 250 nM (Fig. S3) because high substrate DNA density greatly disturbed the hybridization due to steric effects and low density strongly decreases the binding affinity of the substrates to their complementary DNAs. As a result, 250 nM substrate DNA and the

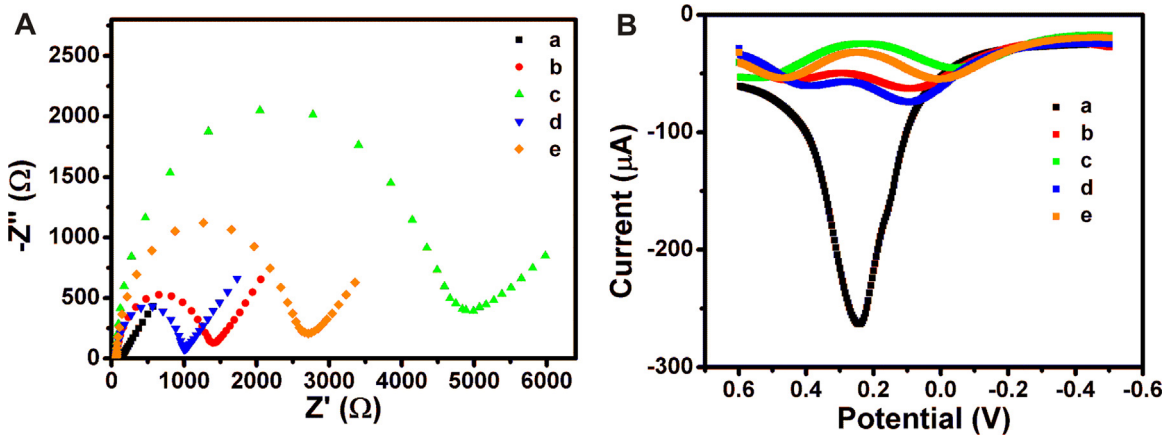

Fig. 2. The stepwise fabrication process of the aptasensor monitored by EIS and SWV. Nyquist plot (A) and the SWV curve (B) of bare gold electrode (a), modified substrate and MCH (b), incubation with 1 ng mL^{-1} CEA (c), presence of Zn^{2+} (d) and incubation with PAA/Link nanogel (e). EIS was measured in 0.1 M KCl with 5 mM $[Fe(CN)_6]^{3-/4-}$ at the open circuit potential. SWV was conducted in 0.1 M KCl with 5 mM $[Fe(CN)_6]^{3-/4-}$ and in range from 0.6 to −0.5 V with modulation amplitude of 25 mV.

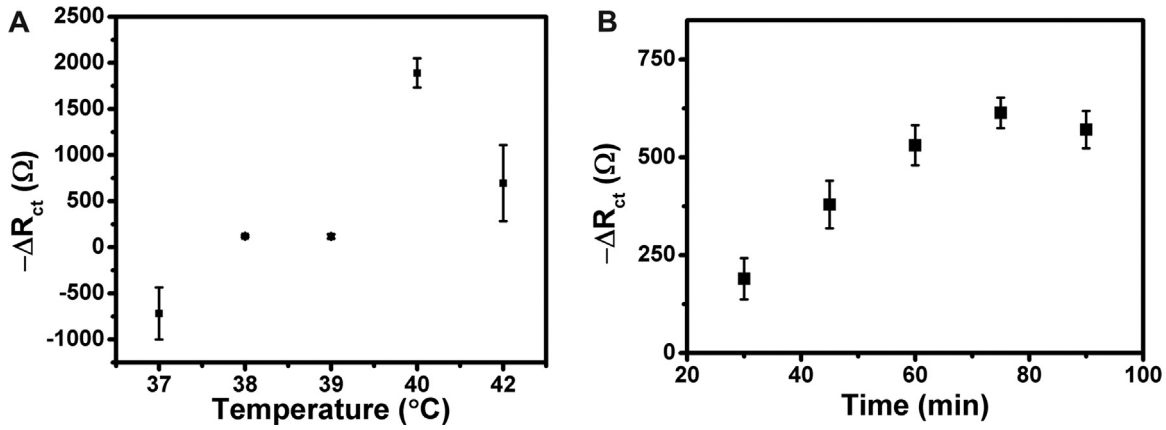

Fig. 3. Effects of cleavage temperature (A) and recycling time on EIS responses (B). ΔRct = R′-R$_0$′; R′ and R$_0$′ denote the charge transfer resistance with or without target in the absence of PAA/Link nanogel, respectively. The data are averages of three individual experiments.

corresponding concentration of aptamer-enzyme DNA were selected for the following experiments.

The cleavage temperature and recycling time were indispensable factors influencing the stability and sensitivity of the recycling reaction (Fig. 3). To attain the desired recycling reaction, these factors were investigated using EIS. The optimum cleavage temperature of 40 °C was taken into account for the recognition and cleavage rate (Fig. 3**A**). The -ΔR_{ct} value was augmented with increased recycling time and then tended towards plateau after 60 min, which implies that balance is achieved between the cleavage and hybridization (Fig. 3**B**). The RSDs of 30, 45, 60, 75 and 90 min were determined to be 17.4%, 16.1%, 9.6%, 6.4% and 8.4%, respectively, which elucidated that prolonged recycling time was beneficial to the measurement stability and repeatability. Consequently, a recycling time of 60 min was chosen for subsequent experimentation.

3.6. Performance of aptasensor for detecting CEA

The equivalent circuit of the aptasensor was obtained by fitting the Nyquist plot via the EC-Lab software (Fig. 4**B**). In the equivalent circuit, the double-layer capacitance CPE results from the charge being stored in the double layer at the interface. The Warburg impedance (W) is caused by the impedance of the current due to diffusion from the bulk solution into the interface. Rs is the solution resistance afforded by the ion concentration and the cell geometry, and the charge transfer resistance R_{ct}, which corresponds to the diameter of the semicircle in the Nyquist plot (Fig. 4**A**), refers to the current flow produced by redox reactions at the interface. Fig. 4**A** showed that the R_{ct} values gradually decreased with increasing CEA concentrations over the range of 10.0 fg mL^{-1} to 10.0 ng mL^{-1}. The -ΔR_{ct} values were directly proportional to the logarithm of CEA concentration. The regression equations were determined to be -ΔR = 814.6lgC_{CEA} + 2236.7 with a correlation coefficient of 0.994 in buffer solution and -ΔR = 965.7lgC_{CEA} + 3372.7 with a correlation coefficient of 0.995 in human serum (Fig. 4**B**). The -ΔR_{ct} values at each concentration of CEA in human serum were all slightly higher than those in buffer solution, while the slopes of the two calibration curves measured in buffer solution and in human serum were very similar. Five samples were used for the sensitivity test, and the RSD was determined to be 6.44%. The detection limits in buffer solution and human serum, 7.9 fg mL^{-1} and 1.4 fg mL^{-1} respectively, were calculated by three times the standard deviation above the blank. Compared with recently reported aptasensors based on EIS systems for determining CEA, the proposed aptasensor exhibited enhanced sensitivity, a wider dynamic range and shorter analytic time (Table S2).

3.7. Selectivity and stability

The CEA triggers tandem specific recognition and cleavage operations can endow the proposed aptasensor with excellent selectivity based on hairpin DNA design containing the sequence of the CEA aptamer. To verify the fidelity, CEA (1 ng mL^{-1}) and 10 fold concentrations of other proteins, including PSA, NSE and lgG, were investigated by monitoring the change in resistance under identical conditions (Fig. 5). Obviously, only in the presence of CEA, can a huge decrease in resistance be obtained relative to that of blank. Importantly, the resistance change of the mixture containing CEA and above-mentioned

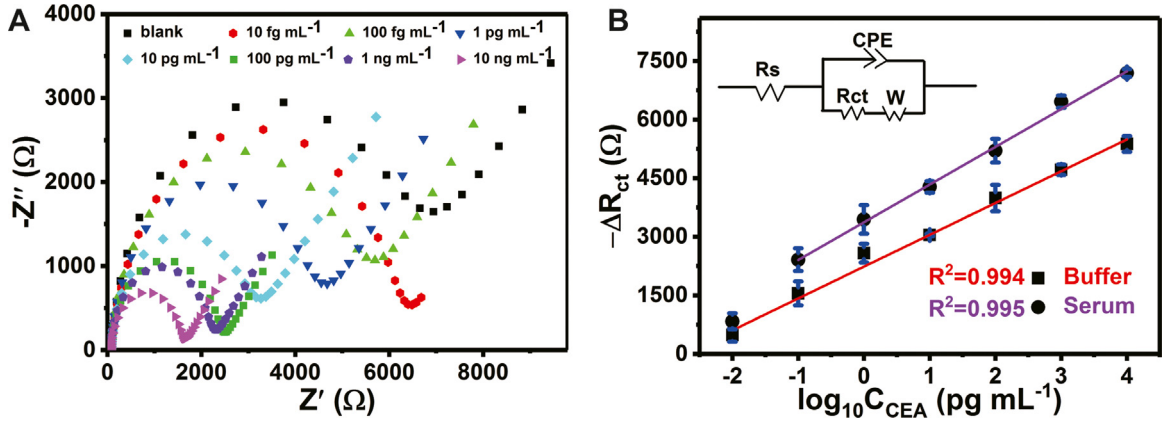

Fig. 4. The nyquist plot (A) and calibration curve (B, ■) for CEA detection in buffer solution. The calibration curve obtained in human serum is shown in B (•) (Insert corresponding the equivalent circuit). Error bars represent standard deviations of three parallel experiments.

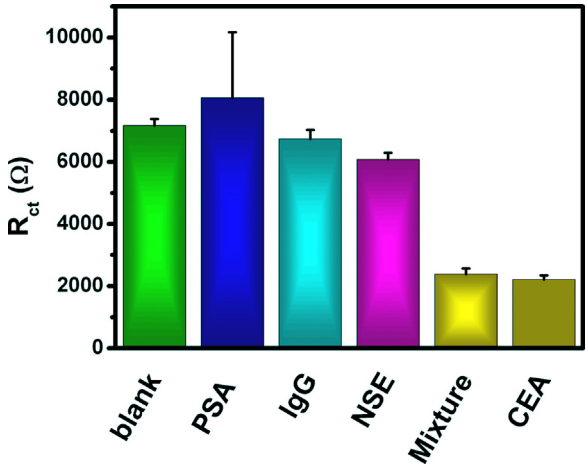

Fig. 5. The selectivity tests of the impedimetric aptasensor for detection of CEA (1 ng mL^{-1}) against other proteins including prostate specific antigen (PSA), human immunoglobulin G (IgG) and neuron specific enolase (NSE) at 10 ng mL^{-1}. The data reported are averages of three parallel experiments.

proteins was similar to that of the CEA, implying that the proposed aptasensor possesses a good specificity for CEA. To further explore the possible applications of the aptasensor in practical use, the stability was assessed. The fabricated aptasensor was stored at 4 °C for two weeks, then EIS was employed to examine its electrochemical response to 1 ng mL^{-1} CEA. Three samples of 1 ng mL^{-1} were used for the stability test, and RSDs of 0.767%, 10.8%, 5.19% of EIS response were obtained after 0, 7 and 14 days, respectively. The EIS response slightly changed to −4.8% after 7 days and then to 4.7% after 14 days in Fig. S4. These results exhibited good stability of the aptasensor.

3.8. Real sample analysis

The assessment of analyzing real samples is one of the most important performances for the aptasensor. Real serum samples were determined in comparison with chemiluminescence immunoassay analyzer (CMIA) (Table S3). The relative errors between the two methods ranged from 1.72% to 9.38%, suggesting that the proposed aptasensor exhibits high accuracy and feasibility for detecting CEA in clinical samples.

4. Conclusion

In summary, a facile impedimetric aptasensor for sensitively detecting CEA is established based on the target-inspired activation of the DNAzyme and amplification effect of the PAA/DNA nanogel. Compared to other analogue aptasensors, the designed aptasensor possesses the distinct characteristics as follows: (1) The aptasensor exhibits a functional nucleic acid design that incorporates target recognition and recycling cleavage to detect CEA by EIS, and shows autonomous tandem ability. Thus, the artful design of the aptasensor ensures good selectivity and sensitivity. (2) The tandem reaction can visibly shorten the analytic time and simplify the operation relative to the multiple additions of reactants and isolation of intermediates or enzymes. One target can activate one DNAzyme that can cleave the multiple substrate of DNAzyme, fulfilling the “one-to-multiple” amplification. (3) The PAA nanogel modified with DNA, which has poor conductivity and negative charge, is implemented as the amplifier to increase the sensitivity of the aptasensor. Overall, the present approach that incorporates the target-inspired tandem reaction is beneficial to prepare in a wide range of electrochemical aptasensors for the ultrasensitive detection of various target of interesting.

Acknowledgements

We are grateful for financial support from the National Natural Science Foundation of China (21673143, 21273153), Natural Science Foundation of Beijing Municipality (2172016, 2132008), High-level Teachers in Beijing Municipal Universities in the Period of 13th Five-year Plan (IDHT20180517) and Capacity Building for Sci-Tech Innovation - Fundamental Scientific Research Funds (025185305000/195).

Declaration of interest statement

The authors declare no conflict of interest.

Appendix A. Supporting information

Supplementary data associated with this article can be found in the online version at https://doi.org/10.1016/j.bios.2018.12.030.

References

Ali, M.M., Li, Y., 2009. Angew. Chem. Int. Ed. Engl. 48, 3512–3515.
Al-Sagur, H., Komathi, S., Khan, M.A., Gurek, A.G., Hassan, A., 2017. Biosens. Bioelectron. 92, 638–645.
Anthony, P.C., Sim, A.Y., Chu, V.B., Doniach, S., Block, S.M., Herschlag, D., 2012. J. Am. Chem. Soc. 134, 4607–4614.
Chandra, P., Noh, H.B., Won, M.S., Shim, Y.B., 2011. Biosens. Bioelectron. 26, 4442–4449.
Chen, Y., Zhou, S., Li, L., Zhu, J., 2017. J. Nano Today 12, 98–115.
Chinen, A.B., Guan, C.M., Ferrerr, J.R., Barnaby, S.N., Merhel, T.J., Mirkin, C.A., 2015. Chem. Rev. 115, 10530–10574.
Choi, S.J., Ban, C., 2016. Sci. Rep. 6, 34998–35011.
Del Bonis-O'Donnell, J.T., Thakrar, A., Hirschberg, J.W., Vong, D., Queenan, B.N., Fygenson, D.K., Pennathur, S., 2018. ACS Chem. Neurosci. 9, 849–857.
Deng, C.Y., Chen, J.H., Nie, Z., Wang, M.D., Chu, X.C., Chen, X.L., Xiao, X.L., Lei, C.Y., Yao, S.Z., 2009. Anal. Chem. 81, 739–745.
Dunn, M.R., Jimenez, R.M., Chaput, J.C., 2017. Nat. Rev. Chem. 1, 0076.
Gao, R.R., Yao, T.M., Lv, X.Y., Zhu, Y.Y., Zhang, Y.W., Shi, S., 2017. Chem. Sci. 8, 4211–4222.
Guo, C.P., Su, F.F., Song, Y.P., Hu, B., Wang, M.H., He, L.H., Peng, D.L., Zhang, Z.H., 2017. ACS Appl. Mater. Interfaces 9, 41188–41199.
Her, J., Jo, H., Ban, C., 2017. Sens. Actuators B-Chem. 242, 529–534.
Lee, S., Manjunatha, D.H., Jeon, W., Ban, C., 2014. PLoS One 9, e100847.
Li, H., Arroyo-Curras, N., Kang, D., Ricci, F., 2016. J. Am. Chem. Soc. 138, 15809–15812.
Li, J.Y., Fu, W.X., Bao, J.C., Wang, Z.Y., Dai, Z.H., 2018. ACS Appl. Mater. Interfaces 10, 6965–6971.
Liu, J.W., Cao, Z.H., Lu, Y., 2009. Chem. Rev. 1948–1998.
Liu, J.W., Lu, Y., 2004. Anal. Chem. 76, 1627–1632.
Liu, R., Yang, Z.H., Guo, Q., Zhao, J.C., Ma, J., Kang, Q., Tang, Y.F., Xue, Y.H., Lou, X.H., He, M., 2015. Electrochim. Acta 182, 516–523.
Mawad, D., Lauto, A., Wallace, G.G., 2016. Conductive Polymer Hydrogels. Springer International Publishing Switzerland, Switzerland.
Chandra, P., 2016. Nanobiosensors for Personalized and Onsite Biomedical Diagnosis. IET, London.
Park, J.Y., Chang, B.Y., Nam, H., Park, S.M., 2008. Anal. Chem. 8035–8044.
Park, J.Y., Park, S.M., 2009. Sensors (Basel) 9, 9513–9532.
Ren, X., Ma, H.M., Zhang, T., Zhang, Y., Yan, T., Du, B., Wei, Q., 2017. ACS Appl. Mater. Interfaces 9, 37637–37644.
Schlosser, K., Li, Y., 2010. ChemBioChem 11, 866–879.
Shaik, M.R., Kuniyil, M., Khan, M., Ahmad, N., Al-Warthan, A., Siddiqui, M.R., Adil, S.F., 2016. Molecules 21, 292.
Song, S., Wang, L., Li, J., Fan, C., Zhao, J., 2008. TrAC Trends Anal. Chem. 27, 108–117.
Wang, G.X., Xu, Q.J., Liu, L., Su, X.L., Lin, J.H., Xu, G.Y., Luo, X.L., 2017. ACS Appl. Mater. Interfaces 9, 31153–31160.
Wu, Y.M., Li, G.P., Zou, L.N., Lei, S., Yu, Q., Ye, B.X., 2018. Sens. Actuators B-Chem. 259, 372–379.
Xu, M.D., Gao, Z.Q., Wei, Q.H., Chen, G.N., Tang, D.P., 2015. Biosens. Bioelectron. 74, 1–7.
Yang, X.M., Zhuo, Y., Zhu, S.S., Luo, Y.W., Feng, Y.J., Xu, Y., 2015. Biosens. Bioelectron. 64, 345–351.
Zhai, Q.F., Zhang, X.W., Xia, Y., Li, J., Wang, E., 2016. Analyst 141, 3985–3988.
Zhang, Z., Balogh, D., Wang, F., Willner, I., 2013. J. Am. Chem. Soc. 135, 1934–1940.
Zhao, J.C., Ma, Z.F., 2018. Biosens. Bioelectron. 102, 316–320.
Zhong, X., Lv, J., Xue, S., Yuan, R., Chai, Y., 2018. J. Electrochem. Soc. 165, B223–B226.
Zhou, X.X., Guo, S.J., Gao, J.X., Zhao, J.M., Xue, S.W., Xu, W.J., 2017. Biosens. Bioelectron. 98, 83–90.
Zhou, Z.J., Xiao, L., Xiang, Y., Zhou, J., Tong, A.J., 2015. Anal. Chim. Acta 889, 179–186.